DOWNHOLE SEPARATOR TESTING FOR SUCKER ROD PUMPS APPLICATIONS

Edgar J. Castellon, Eduardo Pereyra, Cem Sarica
The University of Tulsa, Horizontal Wells Artificial Lift Project

Furqan Chaundhry, Ovintiv

Stuart Scott, Conoco

ABSTRACT

Downhole separation is a critical process for proper sucker rod pump operation. This technology has been successfully applied in vertical wells, providing a solution for gas interference. New horizontal wells present a new challenge to this technology, since slug flow is a predominant flow pattern when sucker rod pumps are implemented. Many past experimental studies have examined continuous gas and liquid injection near the separator inlet. In these cases, separators operate continuously, and separation efficiency is primarily measured for vertical position. Thus, there is a need to develop an experimental procedure that accounts for the intermittent operation of the sucker rod pump and the inclination effect.

This paper presents a novel experimental procedure to characterize the performance of downhole separators under the periodic behavior of a sucker rod pump. The paper describes the facility and the measurements. Computer vision algorithms are used to measure the gas void fraction entering the pump and the bubble size distribution. Results for a poor boy are also presented and compared with those for a single dip tube.

INTRODUCTION

The accumulation of liquid in wells poses a significant operational challenge, as it markedly reduces production efficiency. One method used to lift the liquid is the sucker rod pump system (SRP); However, transporting large volumes of liquid with associated gas to the surface remains difficult for these installations. A downhole gas separator can be deployed below the pump intake to remove part of the gas from the produced liquid before it enters the pump (Al Munif et al., 2023). Although gas interference at the pump intake is well recognized, the mechanism governing the presence of free gas remains poorly understood. Consequently, downhole separators are frequently installed in configurations that may be ineffective, or even detrimental, to overall pumping performance (McCoy et al., 2007).

Downhole separators are generally classified by separation mechanism as centrifugal, gravity-driven, or hybrid. Centrifugal separators may be further categorized as dynamic

or static (Dastyar et al., 2023). In addition, the periodic motion of the SRP introduces unsteady flow conditions that influence separation performance in ways not captured by steady-state assumptions. This study evaluates the separation behavior of gravity-type separators under the cyclic action operating conditions characteristic of sucker rod pumping systems.

Figure 1 illustrates a poor boy (gravity-driven) downhole separator installed below a pump. The separator's outer barrel or mud anchor (inverted shroud) has entry ports through which the produced liquid and a portion of the free gas enter the device. Inside the shroud, a smaller-diameter dip tube conveys the separated liquid into the pump. The annular region between the shroud and the dip tube (separation area) is occupied by a gas-liquid mixture, within which the gas-free liquid flows downward into the dip tube section. Finally, the less dense gas phase in the mixture rises through the liquid at a velocity relative to the liquid due to buoyancy. Depending on the individual gas bubbles' slip velocity, some bubbles are entrained downward by the liquid into the dip tube, while others rise and exit through the same entry ports the liquid initially used to enter the shroud-dip tube annulus, ultimately venting into the casing-shroud annulus (Bohorquez et al., 2007).

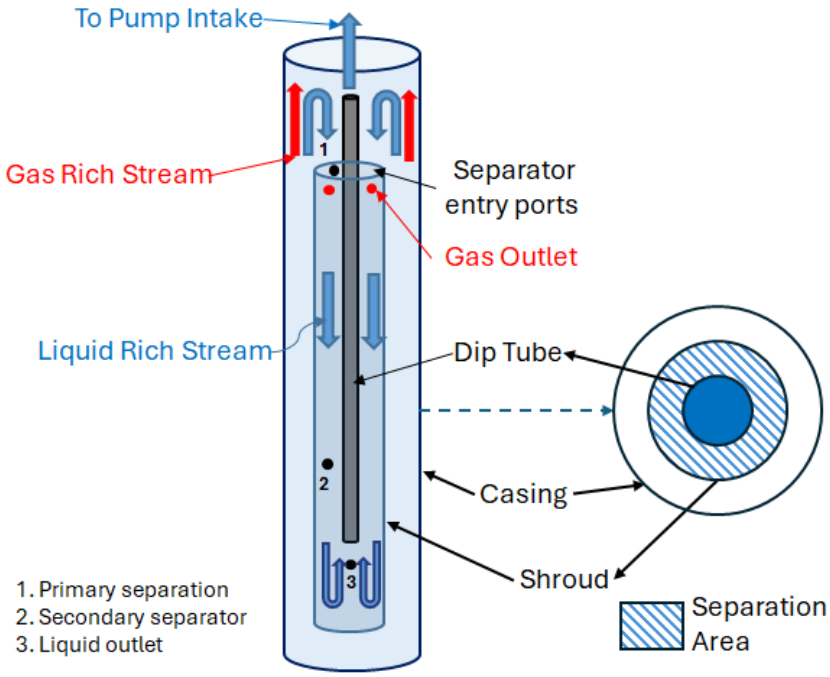

Figure 1 – Gravity-driven downhole separator schematic

Gas removal occurs in two distinct stages (
Figure 1). Primary separation occurs at the entry ports, where most gas disengages and flows upward beyond the casing-shroud annulus. However, a portion of the gas is entrained across the separator entry ports due to high liquid velocity. Secondary separation then occurs within the separation area. A small fraction of the entrained gas

detaches from the downward-moving liquid, escapes through the uppermost row of gas outlets, and returns to the annular space. Nevertheless, the amount of gas separated in this way seems rather low (Ibarra et al., 2013). This secondary separation mechanism is particularly significant in SRP applications because the liquid within the shroud-dip tube annulus becomes stagnant during downstroke. Under these conditions, the drag forces acting on the gas phase are effectively minimized, enabling bubbles to rise with minimal resistance. The extent of this upward migration depends strongly on bubble diameter; smaller bubbles may ascend only a limited distance before the upstroke initiates and the downward liquid motion resumes. These cyclic flow reversals create a residence-time distribution for bubbles within the annulus, ultimately determining whether a given bubble exits the separator via the gas outlet or is carried downward into the dip tube. This aspect has not been considered in common evaluation methodologies for downhole separators used in SRP systems.

Similarly, the cyclic dynamics of the SRP have a substantial influence on the flow rate through the dip tube, represented on Figure 2, neglecting the rod dynamics and other pump effects. The transition from a homogeneous gas-liquid flow to intermittent flow requires a modification in the evaluation approach. This intermittent flow can be characterized by the alternating upstroke and downstroke, each imposing distinct conditions on the fluid circulating within the separator and the dip tube. Consequently, the separation performance cannot be accurately assessed without accounting for the stroke-dependent variations in flow behavior.

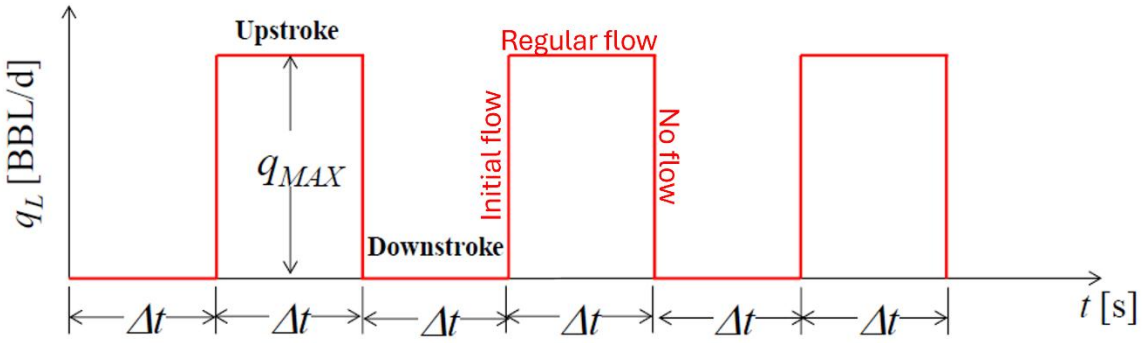

Figure 2 - Downhole separator liquid flow rate behavior for sucker rod pump

The upstroke is characterized by a continuous increase in liquid flow rate until its maximum value (q_{MAX}), which depends solely on the time required for the SRP to displace the total stroke length (Δt). Based on these variables, the average liquid flow rate can be expressed as:

$$\overline{q_L} = \frac{(q_{min}\Delta t + q_{max}\Delta t)n}{(\Delta t + \Delta t)n} . \quad (1)$$

Where n is the number of cycles, and, as the flow rate approaches 0 (q_{min}) during the downstroke, the expression simplifies to

$$q_{max} = 2\overline{q_L}\,. \tag{2}$$

As the flow rate increases during the upstroke, the corresponding liquid velocity and drag force acting on the gas phase also increase. Consequently, a larger fraction of gas is drawn into the shroud-dip tube annulus, compared with conditions in which the flow remains homogeneous. In contrast, the downstroke reduces the flow through both the dip tube and the separator, ultimately decreasing the liquid velocity and the associated drag force to zero. As discussed previously, this is an important contribution towards the secondary separation mechanism. However, in this portion of the cycle, the gas that has already entered the dip tube accumulates as a large gas pocket at the upper end. When the subsequent upstroke begins, these gas pockets are displaced into the region above the standing valve, where they ultimately interfere with pump fillage. Taking this phenomenon into account, it is necessary to establish three flow stages (Figure 2): Initial flow, Regular flow, and No-flow, which can properly characterize the observable changes across each upstroke-downstroke cycle. These will be further discussed in the following section.

Together, these considerations establish the need for an experimental framework capable of capturing the stroke-dependent flow behavior described above, as detailed in the following section.

EXPERIMENTAL FACILITY

This study employs the University of Tulsa Artificial Lift Project (TUHWALP) Inclinable Downhole Separation Facility, which consists of five primary sections: liquid delivery system, gas delivery system, downhole separator, casing gas outlet, and liquid return line. The facility is designed to operate at various deviation angles, ranging from vertical to fully horizontal, by attaching a mechanical boom to sections 3,4, and 5 (downhole separator, gas casing outlet, and liquid return line). A schematic representation of the facility is shown in Figure 3.

Section 1 (liquid delivery system) consists of an 800-gallon storage tank and Seepex® BW5 and Tarby® 107CDQ progressive cavity pumps, connected in parallel through a ¾-in pipe, with a maximum capacity of 45 GPM at a maximum pressure of 45 psig. This system is supplied with tap water from the City of Tulsa. Section 2 (gas delivery system) receives compressed air from a 20 hp Gardner Denver® dry-rotary screw-type compressor through a 2 in airline with a capacity of 1050 SCFM at 100 psi. Airflow rate is measured using an Endress+Hauser® Promass 83F Coriolis mass flow rate meter, followed by a control valve connected to a PI controller that manages the mass flow rate.

Along section 3, several cameras (Figure 3), were installed to record flow behavior at different points of interest, such as upstream to the separator (camera 5), at the inlet of the shroud (camera 4), for liquid level monitoring (camera 3), before the quick closing valve or QCV-1 (camera 2), and after QCV-1 (camera 1). Section 3 is subdivided into the development region, the downhole separator region, the casing, and the separator liquid outlet (tubing). The development section is a 3-in ID, 15 ft long acrylic pipe that allows

the flow to develop before the separator. A pressure transmitter and conductivity probes located at the end of the region monitor and characterize the flow behavior upstream of the separator. The downhole separator region comprises a 6-in casing, which contains a 4-in ID by 75-in long shroud and a 2-in ID tailpipe extending into the liquid return section. The separator liquid outlet consists of a 2-in ID by 30 ft long acrylic pipe, positioned 7 in above the shroud base. At the top of this region, a pair of conductivity probes (CP) and two quick-closing valves (QCV) are installed. The CPs measure the gas void fraction of the mixture entering the pump intake. However, this method is primarily effective for bubbles larger than approximately 7 mm. For smaller bubbles, a computer vision (CV) algorithm has been developed to calculate the gas void fraction and detect bubble size from video recordings downstream of QCV 1. Representative results of this method are shown in Figure 4.

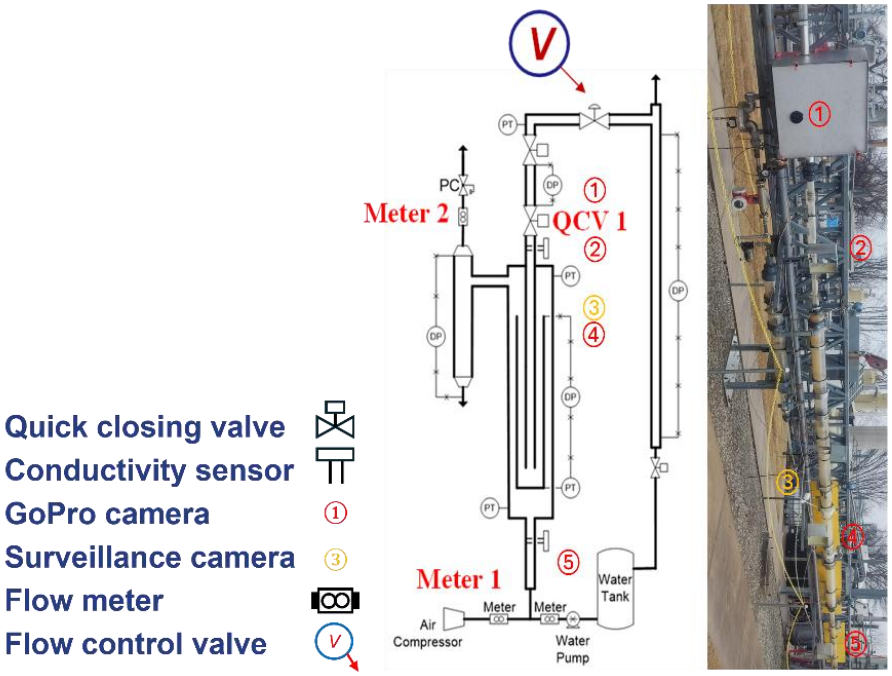

Figure 3 - Facility schematic

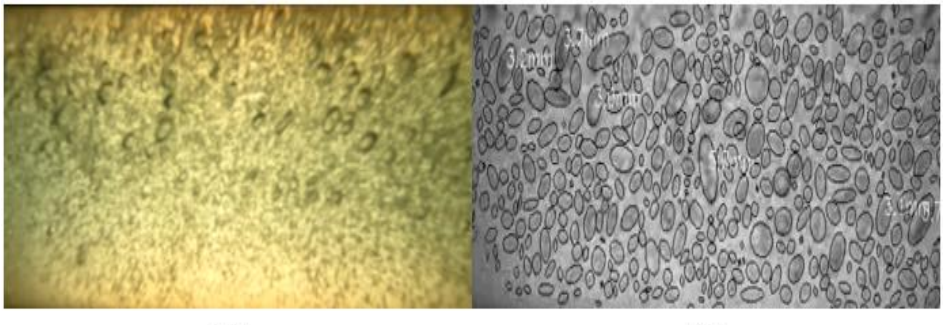

(a) (b)

Figure 4 - Computer Vision (a) original video (b) bubble detection

To simulate the cyclic action of a sucker rod pump, QCV 1 can be programmed to actuate at prescribed intervals (frequency) with the valve opening representing the upstroke and valve closure representing the downstroke. This operation produces three characteristic flow stages (Figure 5). During the no-flow stage, QCV-1 remains closed, and all the non-separated gas accumulates in front of the valve. The instantaneous valve opening causes all of this gas to flow along with the liquid (initial flow), producing the largest gas pockets observed during each test and irregularly sized bubbles. Approximately 2 seconds after the initial flow, the system stabilizes, and bubbles reach a uniform size until the next cycle; this period is defined as regular flow.

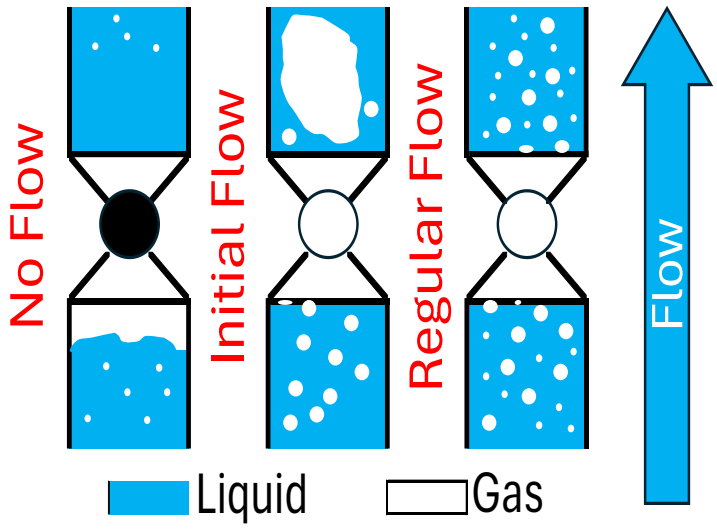

Figure 5 - Flow stages

The gas outlet casing (section 4) is located on the side of section 3. It consists of an additional separator to remove any remaining liquid after the downhole separator. The separated gas stream is measured by an Endress+Hauser® Promass 83F Coriolis mass flow meter, identical to the instrument used in section 2. By using identical flow meters at both the gas inlet and outlet, a proper measure of separation efficiency can be obtained using the following definition.

$$\eta = \frac{\int_{t_{initial}}^{t_{final}} q_{meter2(t)}\, dt}{\int_{t_{initial}}^{t_{final}} q_{meter1(t)} dt} \quad . \tag{3}$$

It is important to note that although this definition provides a useful indication of separation efficiency, it does not represent the actual conditions experienced by the SRP. For this reason, the previously described CV algorithm can be used to estimate the liquid fraction (or holdup) inside the tubing at the pump suction (after QCV 1). This enables the estimation of pump fillage.

Finally, section 5 (liquid return line) consists of a 2-in ID acrylic pipe that directs the separated liquid back to the storage tank. A control valve is installed along this line to regulate the liquid level in the system, ensuring that the shroud remains fully submerged during operation.

EXPERIMENTAL MATRIX

This study considered three base cases (Table 1) to evaluate the impact of the separation area (annular area between dip tube and the shroud) on separation, and in consequence, pump fillage, each with different shroud-tubing configurations.

Table 1 - Base Cases Configurations.

Separator	Base Case 1 (BC1)	Base Case 2 "No Shroud Case" (BC2)	Base Case 2 (BC3)
Tubing ID [in]	2	2	1
Shroud ID [in]	4	-	3
Shroud Length [in]	74	-	74
Schematic	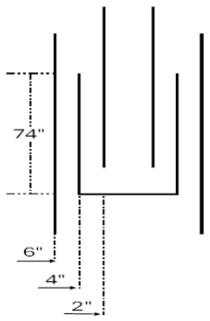	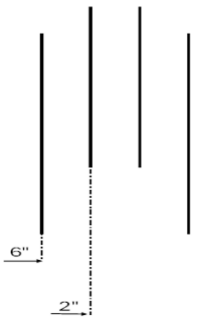	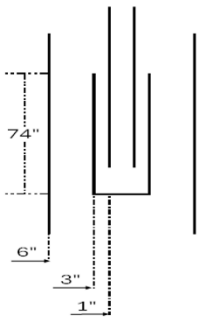

Additionally, this study considered four liquid flow rates (q_L), four gas-liquid ratios (GLR), 2 stroke frequencies (fSR) and three deviations from 0° to 30° as detailed in Table 2.

Table 2 – Experimental matrix.

fSR 3 and 7 [str/min]	Angle	0			Angle	10			Angle	30		
q_L [BPD] \ GLR [scf/bbl]	600	1200	1800	3000	600	1200	1800	3000	600	1200	1800	3000
100			✓	✓		✓	✓				✓	✓
250	✓	✓	✓	✓		✓	✓		✓	✓	✓	✓
400	✓	✓	✓			✓	✓		✓	✓	✓	
500	✓	✓	×			✓	×		✓	✓	×	

Initially, a frequency of 10 strokes/min was tested for BC1; however, it was later removed from the experimental matrix due to its low effect and to allow testing the other cases. The tests without green checkmarks could not be completed due to operational limitations of the facility. Particularly at low gas-liquid ratios (600 and 1200 scf/bbl at 100 BPD) and at high-rate conditions (3000 scf/bbl and liquid rates exceeding 400 BPD).

For each completed test, the acquired data consists of:

- Low-speed data (~1 Hz): Pressure, temperature, differential pressure, gas, and water flow rate.
- High-speed data (~1000 Hz): Conductivity measurements obtained through conductivity sensors.
- Video recordings.
    - GoPro cameras → Axial visualization and bubble detection.
    - Surveillance camera → Liquid level control.

EXPERIMENTAL RESULTS

Flow Rate Effect:

The following results are for efficiency and holdup, both expressed as functions of liquid flow rate and gas-liquid ratio (GLR) for base case 1 (Figure 6) and all base cases (Figure 7). As mentioned previously, Figure 6(a), and Figure 7(a) correspond to measurements from the gas flowing through the gas casing outlet (section 4), on the other hand, Figure 6(b) and Figure 7(b) are based on the liquid flow downstream of the separator (section 5).

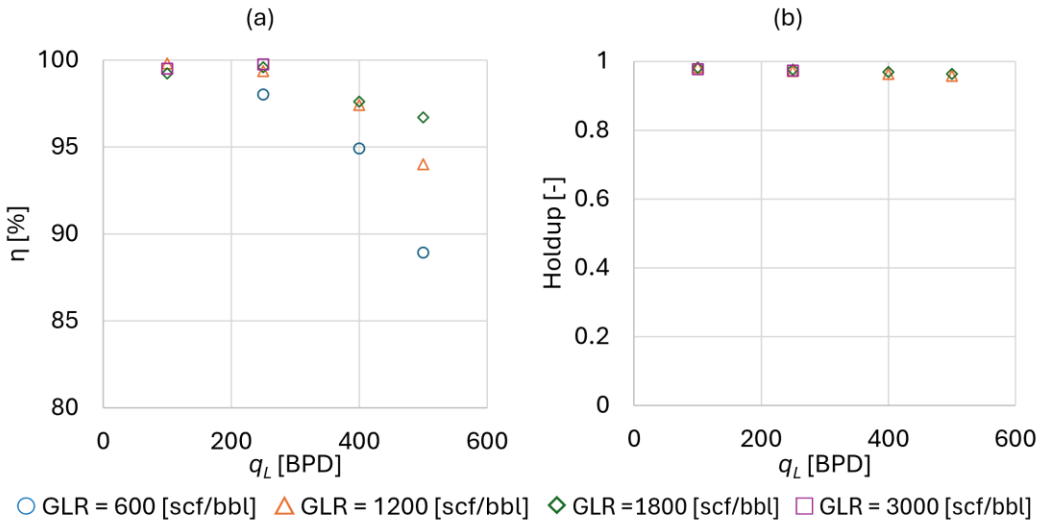

Figure 6 – Separation results for BC1 at 0° and 3 str/min for (a) efficiency and (b) holdup

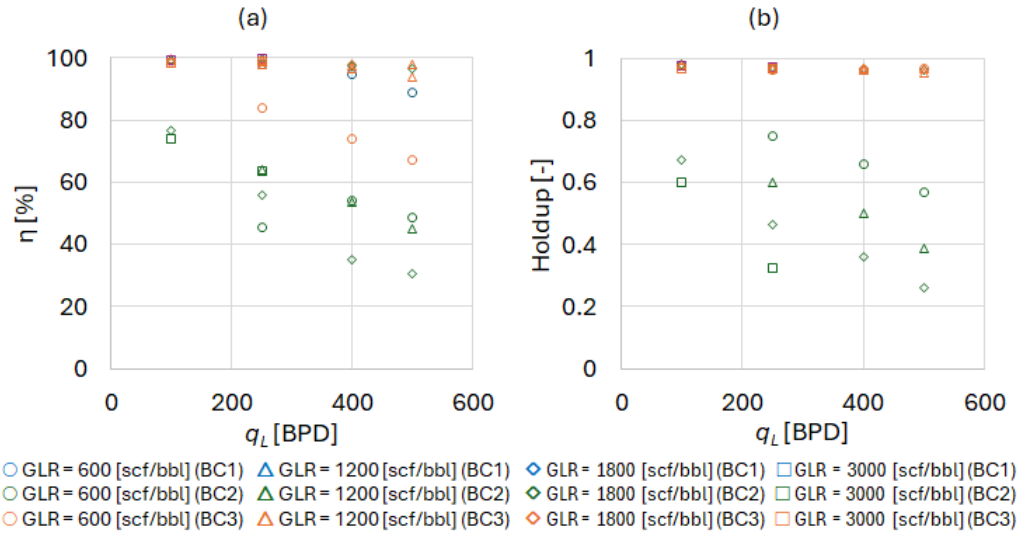

Figure 7 - Separation results at 0° and 3 str/min for (a) efficiency and (b) holdup

Experimental results present consistently high separation efficiency and liquid holdup for low liquid flow rates (<400 BPD). Figure 6(a) and Figure 6(b) show a slight decline in separation performance, inversely related to liquid flow rate (q_L), that becomes noticeable around 400 BPD. Additionally, separation efficiency increases modestly with GLR, particularly at 0° (Figure 6(a)), indicating that, as the gas flow rate (q_G) increases, pump fillage does not exhibit any significant change.

Figure 7 presents the separation results for all base cases. BC1 and BC3 exhibit very similar trends in efficiency and holdup as functions of q_L; however, BC1 shows a slight performance advantage at low q_L attributable to its larger separation area. In contrast, BC2 displays the opposite behavior with respect to GLR when compared with BC1 and BC3: in the absence of an inverted shroud, higher GLR leads to reduced separation efficiency and holdup. This occurs because, without an inverted shroud directing the gas above the dip tube inlet, it flows straight into the dip tube with minimal lateral separation (Figure 8(b)). As a consequence of this same mechanism, BC2 also exhibits the largest gas pockets or Taylor bubbles observed during the initial flow and regular flow stages (Table 3).

Table 3 – Flow stages at 250 [BPD] and 600 [scf/bbl]

Downhole Separator	Initial flow	Regular flow	No flow
Base Case 1	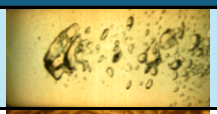		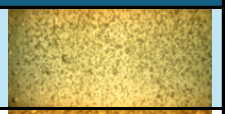
Base Case 2	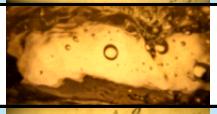	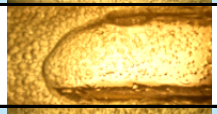	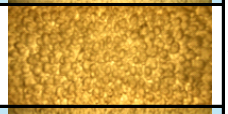
Base Case 3	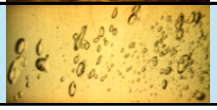	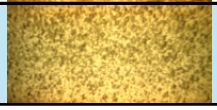	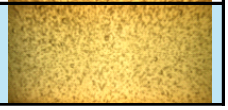

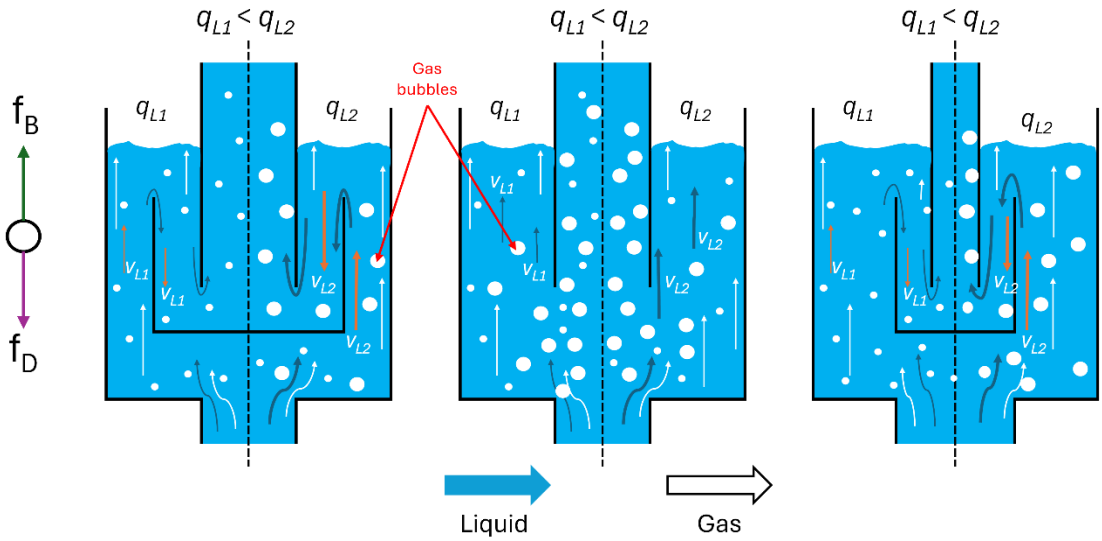

Figure 8- Flow schematic (a) BC1, (b) BC2 and (b) BC3

Separation performance is strongly influenced by both the liquid flow rate (q_L) and the deviation angle. At low q_L (<400 BPD), most of the gas is effectively separated before entering the inverted shroud. At higher q_L, however, a clear decline in efficiency emerges, producing two distinct operational regimes: a high-efficiency region at low flow rates and a low-efficiency region at elevated flow rates. At flow rates above approximately 400 BPD, separator performance decreases linearly with increasing q_L, consistent with observations reported by Ibarra et al. (2013). Furthermore, Lopez et al. (2019) indicate that the transition between these two regions is due to increased drag forces, resulting from higher liquid velocities. The instant liquid changes its flow direction at the shroud inlet, these forces exceed the buoyancy forces acting on the bubbles, enabling the liquid to pull larger gas bubbles into the inverted shroud, as illustrated in Figure 8.

It is important to note, however, that not all the gas entering the shroud ultimately reaches the dip-tube. A portion of it is displaced by secondary separation due to the action of QCV-1 during the no-flow stage, which temporarily halts liquid motion inside the inverted shroud.

Overall, the results demonstrate that separation behavior is fundamentally controlled by the interplay between liquid velocity, drag forces, and shroud geometry, all of which evolve cyclically throughout SRP operation.

Stroke Frequency Effect:

Figure 9 illustrates the impact of increasing the number of cycles per minute (stroke frequency [str/min]), on separation efficiency and holdup, presented as functions of q_L and GLR.

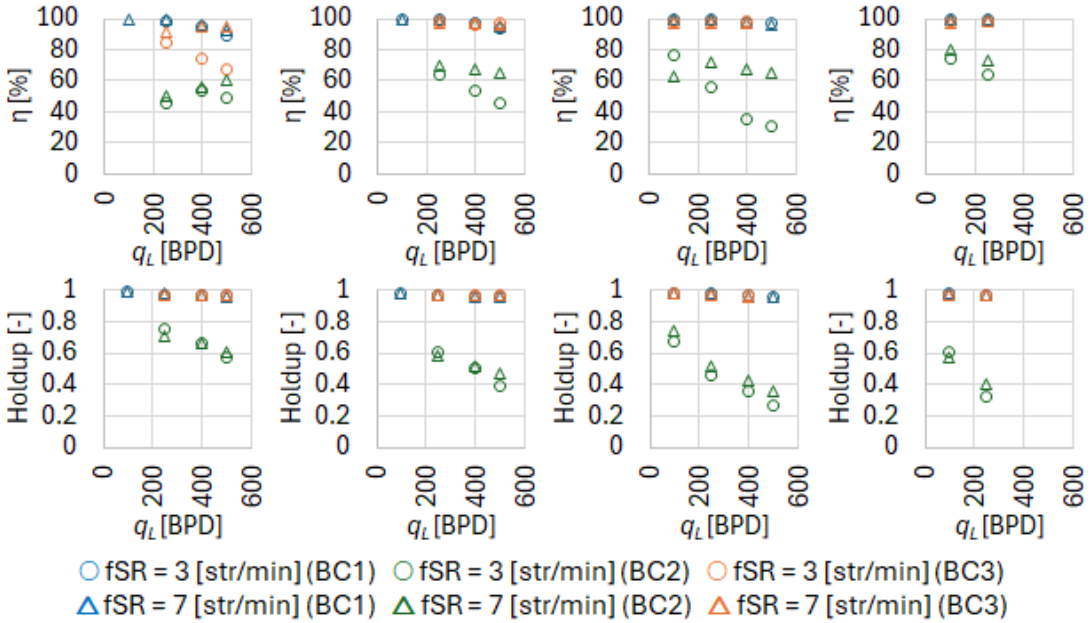

Figure 9 - Frequency effect at GLR (a) 600 [scf/bbl], (b) 1200 [scf/bbl], (c) 1800 [scf/bbl], and (d) 3000 [scf/bbl].

These results indicate that increasing the stroke frequency does not significantly affect separation performance for configurations equipped with an inverted shroud. Nevertheless, for cases such as BC2, where no shroud or secondary separation volume is present, a larger stroke frequency results in higher efficiency, but the liquid fraction is less sensitive to this parameter.

Deviation Effect:

According to Rosli et al. (2024), increasing the deviation angle shifts the transition boundary between the high and low efficiency regions towards a higher liquid flow rate, effectively extending the range of q_L over which the separator maintains strong performance. This trend can be observed in Figure 10, where the overall performance of all separators at 30° is considerably higher than what is observed at 0°. The influence of deviation is particularly notable for BC2: at 30º, its separation performance approaches that of BC1 and BC3 at low q_L. However, this improvement is confined to the lowest q_L (<250 BPD) representing only a narrow portion of the operational envelope.

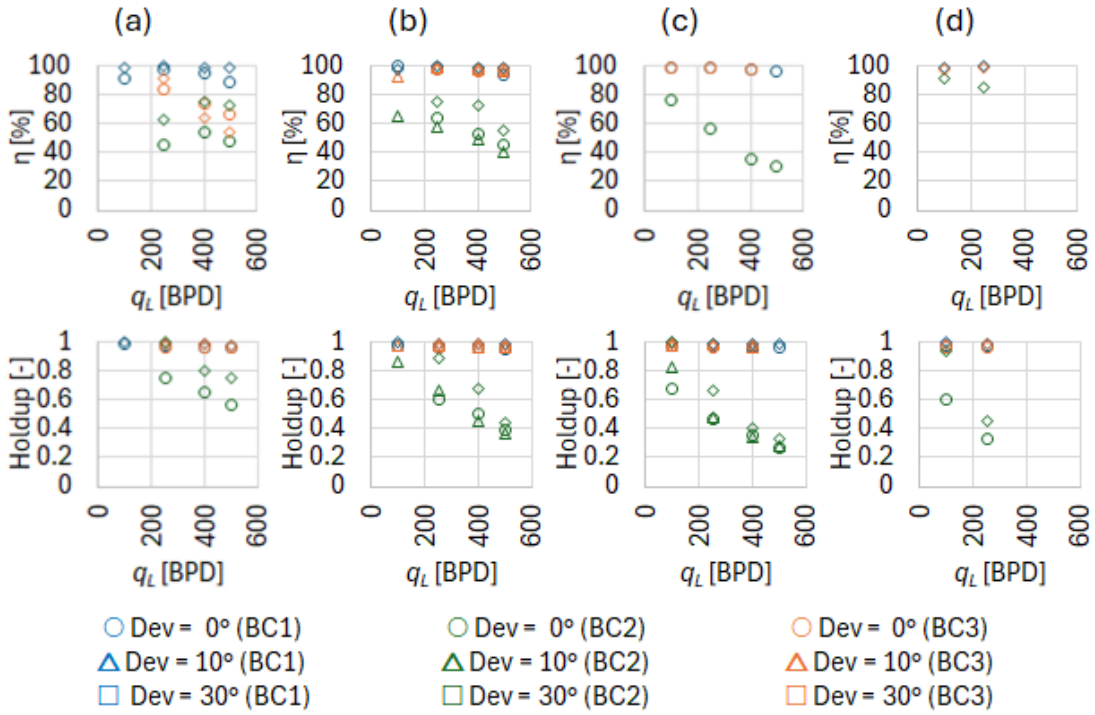

Figure 10 – Deviation effect at (a) 600 [scf/bbl], (b) 1200 [scf/bbl], (c) 1800 [scf/bbl], and (d) 3000 [scf/bbl].

For a deviation angle of 30°, the transition is located at approximately 250 BPD, whereas at 0° it occurs at q_L higher than 400 BPD. As explained in Serrano (1999) and Lopez et al. (2019), this behavior arises from changes in the two-phase mixture configuration (see flow pattern in Figure 11). At high deviations, the gas phase tends to concentrate at the upper section of the annular space between the casing and the inverted shroud. This promotes primary separation upstream of the separator inlet while simultaneously reducing the contact area between the liquid and gas phases, thereby significantly reducing the likelihood that the liquid will drag gas into the shroud.

(a) (b)

Figure 11 – Two-phase mixture configuration (a) 0° and (b) 30°.

Overall, these findings confirm that the deviation angle plays a decisive role in shaping the flow configurations and, consequently, the system's separation performance.

Shroud-tubing Area Effect:

To study the influence of the shroud-tubing area on overall performance, this study has considered 3 base cases (Table 1). Although BC1 and BC3 have the same spacing between the shroud and the tubing, the total area is smaller in BC3. Conversely, removing the inverted shroud in BC2 enables the observation of the influence of a no-shroud case in separation, as shown in Figure 7, Figure 9 and Figure 10. This results in a separation performance ranging from approximately 20 to 80%, even at the lowest q_L condition.

Figure 12 compares BC1 and BC3. In most conditions, BC1 performs slightly better, suggesting that the increased area improves separation by reducing drag forces due to lower liquid velocities within the separator. However, it is important to note that although the separation area in BC3 is smaller than BC1, the annular space between the inverted shroud and dip tube is the same for both cases. This suggests that future studies should further investigate the role of this internal geometry in governing separation behavior.

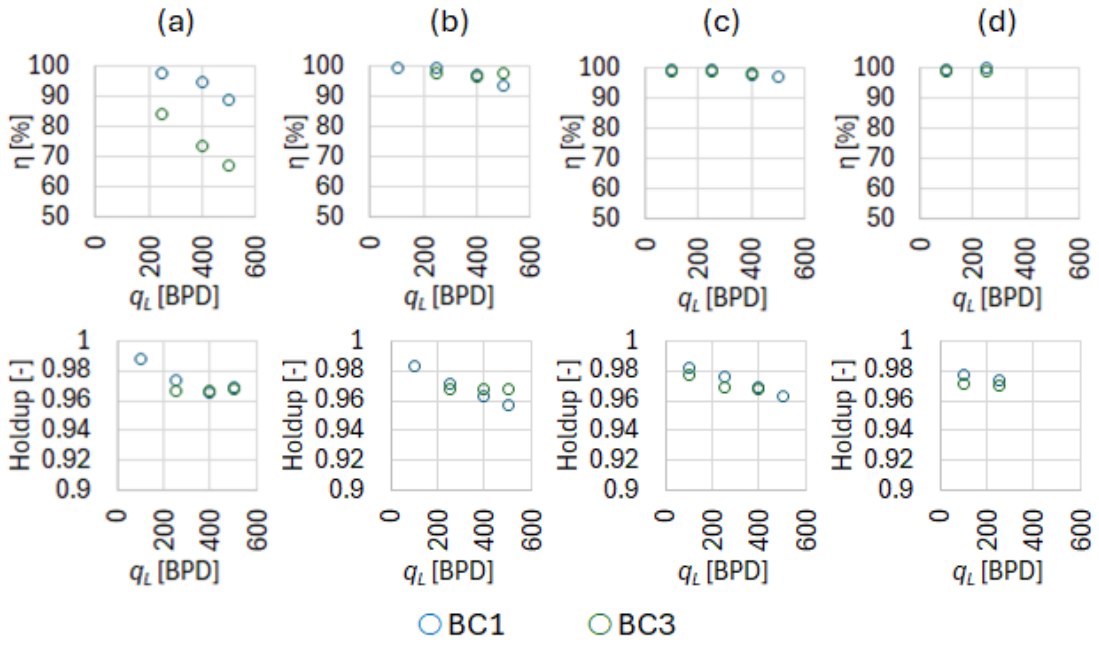

Figure 12 – Separation area (a) 600 scf/bbl, (b) 1200 scf/bbl, (c) 1800 scf/bbl, and (d) 3000 scf/bbl.

These observations confirm that while increased separation area enhances performance, the internal geometry, especially the shroud-dip tube annulus, remains a critical factor that warrants further investigation.

Bubble Size:

As previously discussed, the separation performance downstream of the separator was evaluated using a bubble-detection algorithm developed in OpenCV. The Sauter mean diameter, d_{32}, was selected as the primary metric for bubble size because it is the most commonly used parameter for characterizing liquid–liquid and gas–liquid dispersions. It effectively relates the interfacial area of the dispersed phase to its volume (Pacek et al., 1998). The Sauter mean diameter is defined by the following equation:

$$d_{32} = \frac{\sum n_i d_i^3}{\sum n_i d_i^2} \quad . \tag{4}$$

This approach allows analysis of the liquid phase along with any remaining entrained gas. Just as with separation efficiency, it is essential to evaluate bubble size under the same operating conditions (flow rates, frequency, and deviation). The following figure shows the bubble-size distributions obtained for vertical flow at 3 str/min.

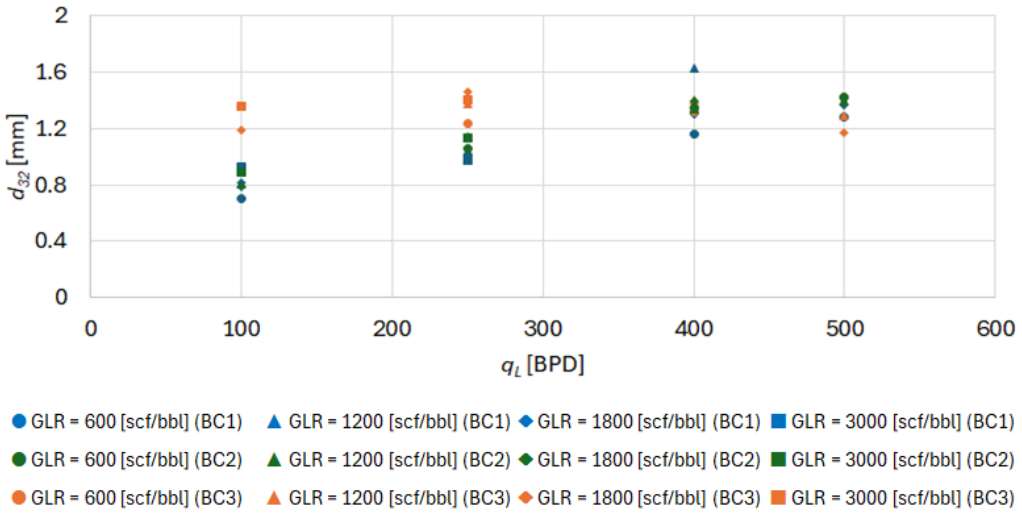

Figure 13 – Bubble detection at 0° and 3 str/min

First, Figure 13 indicates that BC2 produces considerably larger bubbles that remain constant regardless of changes in gas or liquid flow rates. In contrast, BC1 and BC3 produce noticeably smaller bubbles, particularly at low liquid flow rates ($q_L < 400\ BPD$). These bubbles grow as the liquid flow rate increases, reaching sizes comparable to those observed in BC2. Across all configurations, however, the influence of GLR on bubble size is minimal.

A comparison between BC1 and BC3 indicates that, under vertical conditions, bubble size is independent of separation area. The effect of frequency on bubble size, however, can be assessed by comparing 7 str/min (Figure 14) and 3 str/min (Figure 13). Both figures exhibit similar trends with respect to liquid flow rate and separator dimensions, with only a slight increase in bubble size, particularly for BC2. However, the difference between the two is considerably small and therefore considered operationally insignificant.

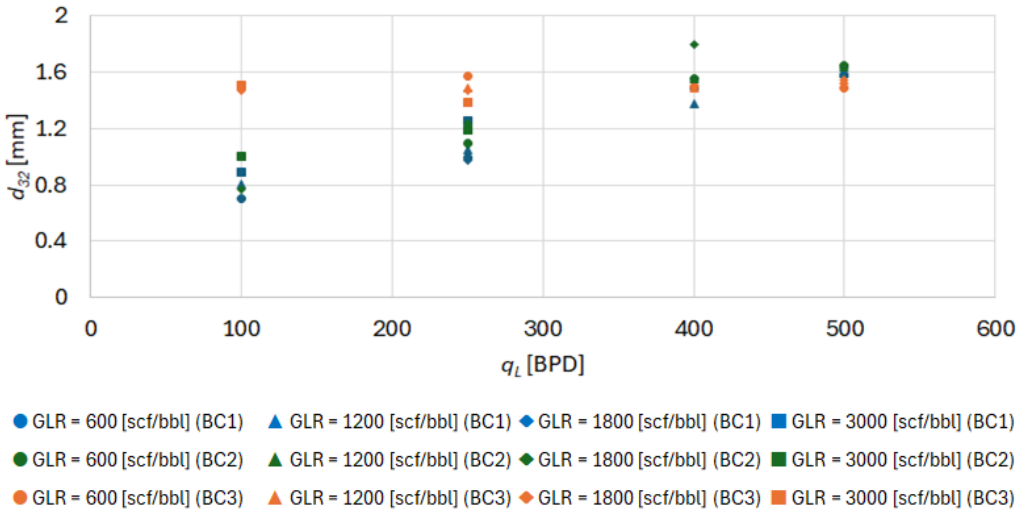

Figure 14 – Bubble detection at 0° and 7 str/min

Finally, Figure 15 presents similar bubble-size trends at 30º that resemble those observed at 0º with respect to flow rates, separation area, and stroke frequency. However, higher deviations clearly lead to smaller bubbles across all conditions. Notably, BC3 shows a nearly constant bubble size across all liquid flow rates, similar to BC2. This suggests a dependency of bubble size with respect to separation area and deviation: at higher deviations, it is necessary to consider larger separation areas, particularly at low q_L to ensure the formation of the smallest possible bubbles.

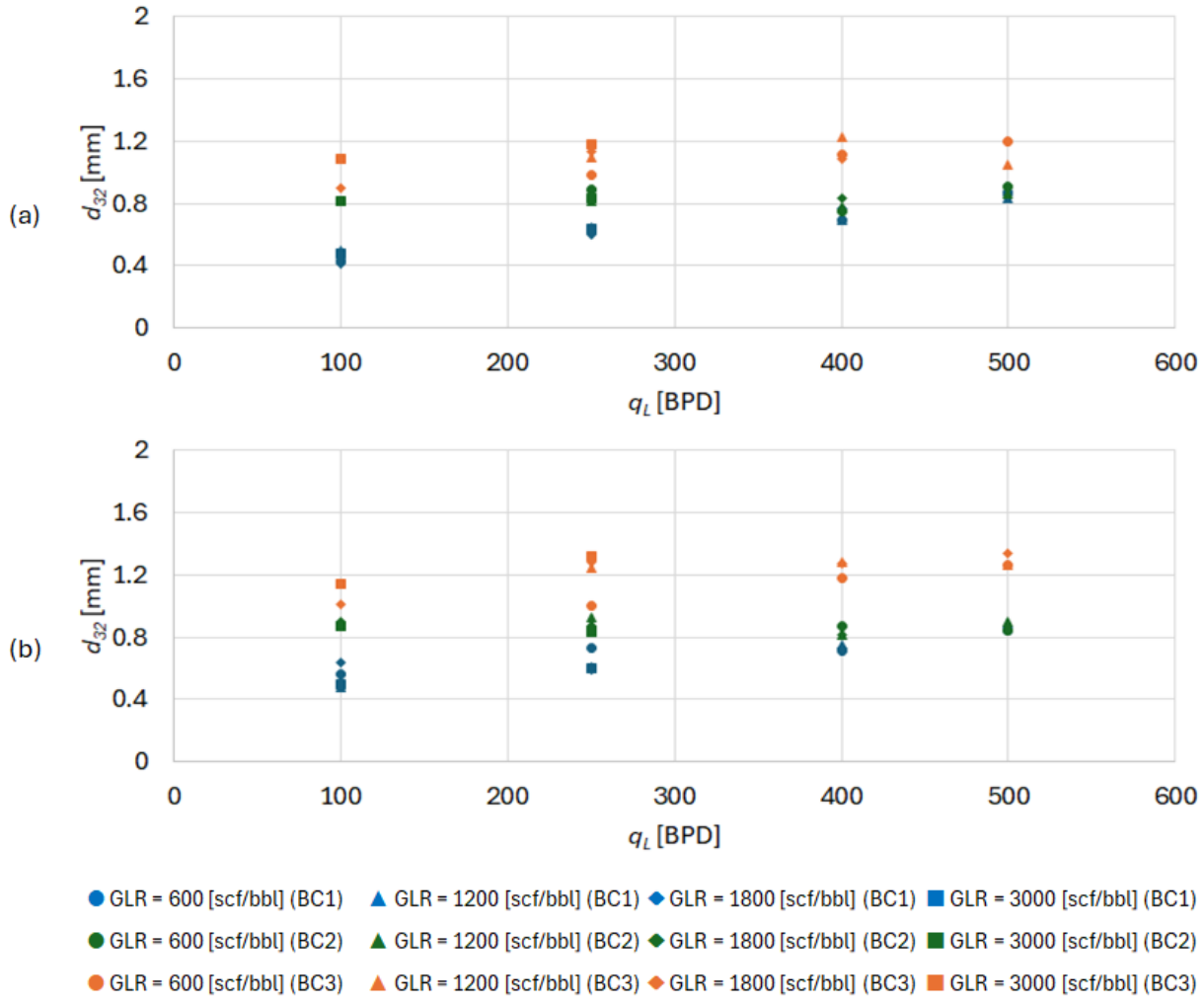

Figure 15 – Bubble detection at 30° at (a) 3 str/min and (b) 7 str/min

As mentioned previously, low-rate conditions result in smaller bubbles; however, the present approach enables the observation not only of bubble size but also of bubble concentration. This distinction becomes evident when comparing Figure 16 and Figure 17 at low operating conditions. Under these conditions, the flow is noticeably clearer, with smaller and more sparsely distributed bubbles for BC1 and BC2, particularly at 30°. In

contrast, high-rate conditions generate not only larger bubbles but also substantially higher bubble concentration.

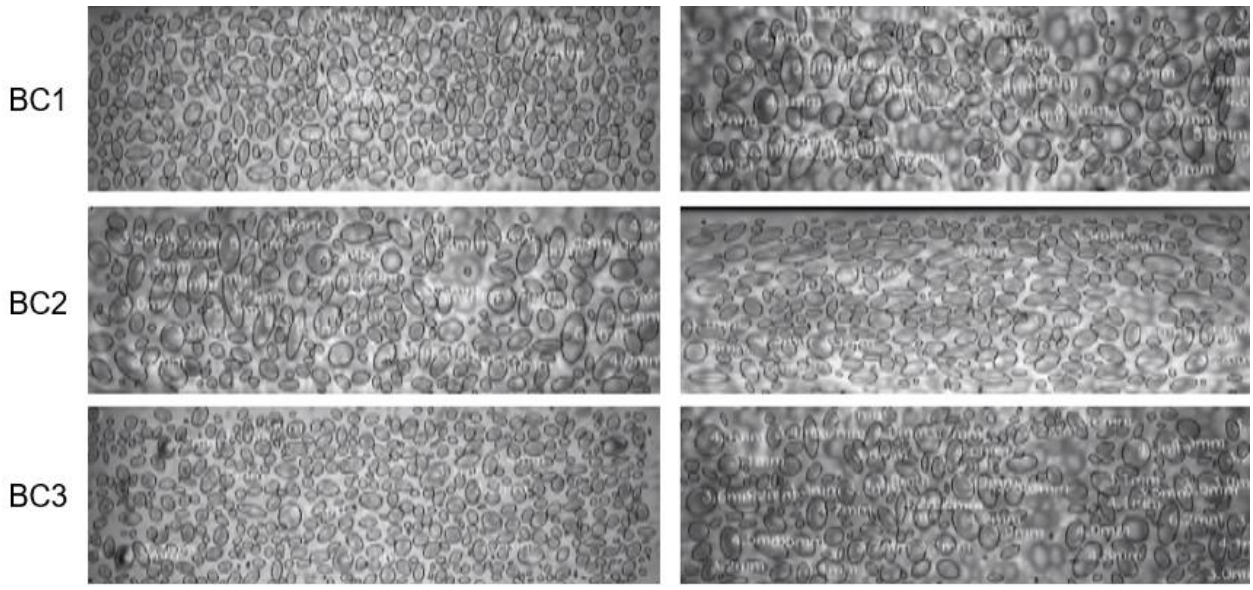

Figure 16 – Bubble size detection 0° for (a) low conditions and (b) high conditions

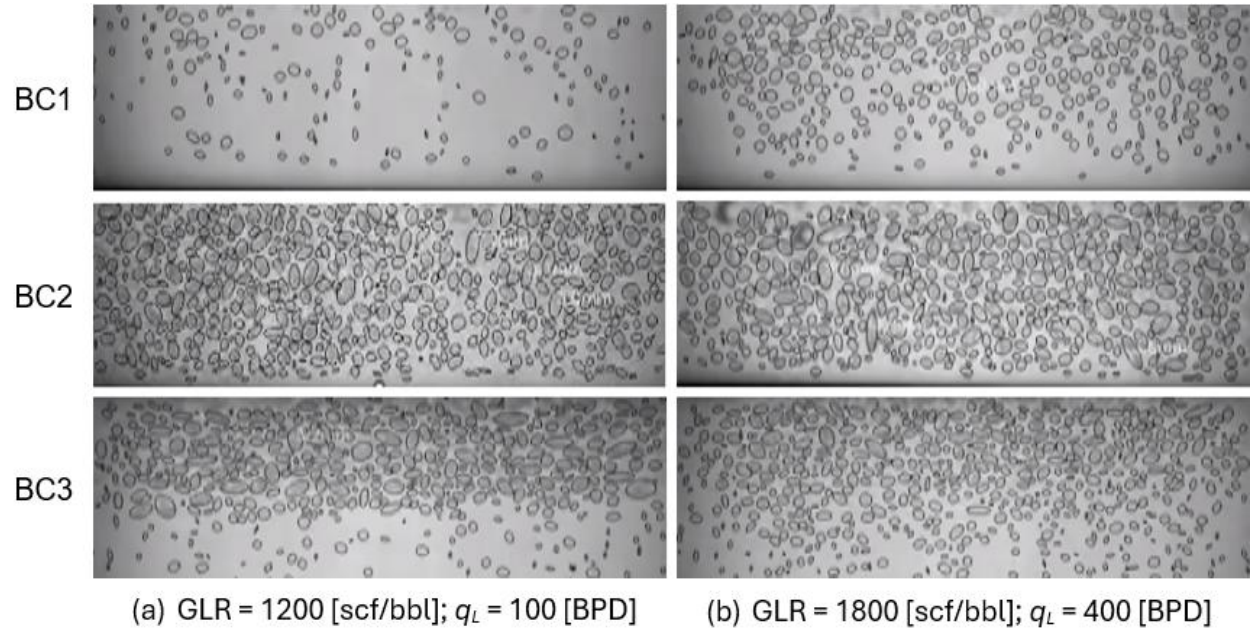

Figure 17 – Bubble size detection 30° for (a) low conditions and (b) high conditions

Collectively, these observations highlight that operating conditions strongly govern bubble size and concentration, and the trends identified here provide essential context for interpreting the broader performance behavior discussed in the previous sections.

CONCLUSIONS

This work introduces a new experimental procedure that explicitly incorporates the intermittent nature of the sucker rod pump operation into the evaluation of downhole separator performance. By capturing the cyclic behavior of the flow, rather than relying on steady-state assumptions, this approach provides a more realistic and more representative assessment of separator behavior under field-relevant conditions. Using this methodology, an extensive experimental study was conducted across a wide range of operational conditions and separator geometries. More specifically, two shroud-type gravity-driven downhole separators with different shroud-dip tube annuli, along with one configuration without a shroud, were tested under numerous gas and liquid flow rates, stroke frequencies, and deviation angles to determine how each parameter influences separation performance. Performance was evaluated from two complementary perspectives: the gas outlet downstream of the separator, representing the conventional definition of separation efficiency, and the liquid outlet downstream of the separator, where computer vision techniques were used to detect and quantify entrained bubbles.

Experimental results indicate two regions of operation, highly influenced by liquid flow rate: a high-efficiency region at liquid flow rates below 400 BPD and a low-efficiency region starting around 400 BPD. A small impact caused by gas flow rate, generally improving separation as the gas-liquid ratio (GLR) increases. Stroke frequency provides a small performance enhancement; however, frequencies above 7 strokes/min do not yield further improvement. In contrast, the deviation angle proves to be the most influential parameter, as greater deviations shift the boundary of the high-efficiency region toward higher liquid flow rates. Additionally, a larger separation area has been shown to improve separation and reduce bubble size by reducing liquid velocity at the separator inlet, thereby enhancing pump fillage. Conversely, the absence of a separation area, as in the no-shroud case, results in consistently low separation across all liquid flow rates with only minimal sensitivity to stroke frequency at low liquid flow rates.

Finally, Bubble size analysis further indicates that, for configurations with a shroud-dip tube annulus (BC1 and BC3), bubbles grow not only in size but also in concentration as the liquid flow rate increases, with insignificant contribution from stroke frequency. In contrast, the lack of an inverted shroud (BC2) exhibits a nearly constant bubble size independent of flow rate. Moreover, high deviation angles reduce bubble size across all tested conditions by promoting gas accumulation along the upper side of the casing upstream of the separator, thereby reducing the effective gas-liquid contact area at the separator inlet.

In summary, the intermittent evaluation procedure developed here represents a significant advancement in the experimental assessment of downhole separators, enabling performance characterization under conditions that more faithfully replicate field operation. By establishing a methodology that captures the true cyclic behavior of SRP systems, this study provides a robust platform for improving separator design, optimizing

artificial-lift performance, and guiding future research toward more field-representative testing practices.

REFERENCES

Al Munif, E. H., Alhamad, L., Ejim, C. E., & Banjar, H. M. (2023). *Review of Downhole Gas Liquid Separators In Unconventional Reservoirs*. SPE Annual Technical Conference and Exhibition. https://dx.doi.org/10.2118/215112-MS

Bohorquez, R., Ananaba, V., Alabi, O., & Podio, A. L. (2007). *Laboratory Testing of Downhole Gas Separators*. https://doi.org/https://doi.org/10.2118/109532-PA

Dastyar, Z., Hajidavalloo, E., & Rabieh, M. M. (2023). *A computational fluid dynamics study for simulation of the unsteady state two-phase flow in vertical separators and plunger pumps simultaneously*. In Review. https://doi.org/10.21203/rs.3.rs-2609250/v1

Ibarra, J., Pardo, R., Vega, L., & Carios, E. (2013). Experimental Study of a Poor Boy Downhole Gas Separator Under Continuous Gas-Liquid Flow. *SPE Artificial Lift Conference-Americas*, SPE-165033-MS. https://doi.org/10.2118/165033-MS

Lopez, J., Pereyra, E., & Sarica, C. (2019). An Experimental Investigation of Dynamic Behavior of Gravity-Driven Downhole Separators. *SPE Annual Technical Conference and Exhibition*, D022S091R002. https://doi.org/10.2118/196197-MS

McCoy, J. M., Patterson, J., & Podio, A. L. (2007). Downhole Gas Separators-A Laboratory and Field Study. *Journal of Canadian Petroleum Technology*, *46*(05). https://doi.org/10.2118/07-05-05

Pacek, A. W., Man, C. C., & Nienow, A. W. (1998). On the Sauter mean diameter and size distributions in turbulent liquid/liquid dispersions in a stirred vessel. *Chemical Engineering Science*, *53*(11), 2005–2011. https://doi.org/10.1016/S0009-2509(98)00068-2

Rosli, R., Pereyra, E., & Sarica, C. (2024). A Detailed Investigation of Gravity-Driven Separation Mechanisms for Horizontal Wells Under Dispersed Flow Conditions. *SPE Artificial Lift Conference and Exhibition - Americas*, D031S009R001. https://doi.org/10.2118/219559-MS

Serrano, J. (1999). *Natural separation efficiency in electric submersible pump systems* [Master's Thesis]. The University of Tulsa.